

# Tropical Cyclone Energy Dispersion in a Three-Dimensional Primitive Equation Model: Upper-Tropospheric Influence\*

XUYANG GE, TIM LI, AND YUQING WANG

*Department of Meteorology, and International Pacific Research Center, University of Hawaii at Manoa, Honolulu, Hawaii*

MELINDA S. PENG

*Naval Research Laboratory, Monterey, California*

(Manuscript received 21 February 2007, in final form 25 October 2007)

## ABSTRACT

The three-dimensional (3D) Rossby wave energy dispersion of a tropical cyclone (TC) is studied using a baroclinic primitive equation model. The model is initialized with a symmetric vortex on a beta plane in an environment at rest. The vortex intensifies while becoming asymmetric and moving northwestward because of the beta effect. A synoptic-scale wave train forms in its wake a few days later. The energy-dispersion-induced Rossby wave train has a noticeable baroclinic structure with alternating cyclonic–anticyclonic–cyclonic (anticyclonic–cyclonic–anticyclonic) circulations in the lower (upper) troposphere.

A key feature associated with the 3D wave train development is a downward propagation of the relative vorticity and kinetic energy. Because of the vertical differential inertial stability, the upper-level wave train develops faster than the lower-level counterpart. The upper anticyclonic circulation rapidly induces an intense asymmetric outflow jet in the southeast quadrant, and then further influences the lower-level Rossby wave train. On one hand, the outflow jet exerts an indirect effect on the lower-level wave train strength through changing TC intensity and structure. On the other hand, it triggers downward energy propagation that further enhances the lower-level Rossby wave train. A sudden removal of the diabatic heating may initially accelerate the energy dispersion through the increase of the radius of maximum wind and the reduction of the lower-level inflow. The latter may modulate the group velocity of the Rossby wave train through the Doppler shift effect. The 3D numerical results illustrate more complicated Rossby wave energy dispersion characteristics than 2D barotropic dynamics.

## 1. Introduction

Investigations concerning the energy dispersion of a barotropic vortex (e.g., Anthes 1982; Flierl 1984; Chan and Williams 1987; Luo 1994; Carr and Elsberry 1995; McDonald 1998; Shapiro and Ooyama 1990; and others) indicate that intense tropical cyclones (TC) are subject to Rossby wave energy dispersion in the presence of the planetary vorticity gradient, the beta effect.

While a TC moves west and poleward because of the beta effect (which induces asymmetric “ventilation” flow over the TC core), Rossby waves emit energy eastward and equatorward. As a result, a synoptic-scale wave train with alternating anticyclonic and cyclonic vorticity perturbations forms in the wake of a TC. Using a nondivergent barotropic model, Carr and Elsberry (1995) noted that the dispersion of a cyclonic vortex involves both linear (beta term) and nonlinear (advection term) processes, and the combination of these two processes determines the wavelength and orientation of a Rossby wave train. Meanwhile, it has been demonstrated that the tropical cyclone energy dispersion (TCED) may affect both the motion and structure of the TC.

Using satellite products from Quick Scatterometer (QuikSCAT), Li and Fu (2006) examined the horizontal structure of a Rossby wave train associated with

---

\* School of Ocean and Earth Science and Technology Contribution Number 7452, and International Pacific Research Center Contribution Number 489.

---

*Corresponding author address:* Xuyang Ge, Department of Meteorology, University of Hawaii at Manoa, 2525 Correa Rd., Honolulu, HI 96822.  
E-mail: xuyang@hawaii.edu

energy dispersion of a preexisting typhoon over the western North Pacific. As the QuikSCAT products provide only the near-surface winds, they cannot reveal the vertical structure of the wave train. Moreover, most previous TCED studies are confined to barotropic dynamical frameworks (Flierl 1984; Chan and Williams 1987; Luo 1994; Carr and Elsberry 1995; and many others). Studies with three-dimensional (3D) models have mainly focused on the TC motion within 3–5 days before significant energy propagation occurs (e.g., Wang and Li 1992; Wang and Holland 1996a,b). Given that in reality a TC has a baroclinic structure with upper-(lower)-level anticyclonic (cyclonic) circulation, and the barotropic model does not include the moist diabatic process, it is important to investigate the TCED in a 3D dynamical framework. In this study, a baroclinic primitive equation model is used to understand the evolution and structure characteristics of the 3D Rossby wave train associated with TCED, with a focus on the connection between the upper- and lower-tropospheric asymmetric circulations. Previous investigators (e.g., Frank 1982; Davidson and Hendon 1989; Holland 1995; Briegel and Frank 1997; Ritchie and Holland 1999; Li et al. 2003, 2006) have suggested that there is a relationship between the TCED and subsequent TC genesis. Therefore, an understanding of the 3D Rossby wave train may give insights into the mechanisms responsible for new TC formation that may help to improve cyclogenesis forecasting capability.

The paper is organized as follows: The model and experimental design are described in section 2. The 3D structure and evolution characteristics of the TCED-induced Rossby wave train are presented in section 3. The generation of the upper-tropospheric asymmetric outflow jet is discussed in section 4. In section 5, the impact of the upper-level outflow jet on the 3D energy dispersion is examined. The role of diabatic heating in forming the Rossby wave train is examined in section 6. Major findings are summarized in the last section.

## 2. Experimental design

### a. Model description

The numerical model used in this study is the uniform grid version of a primitive equation model (TCM3) dedicated for tropical cyclone study. A de-

tailed description of the model can be found in Wang (1999, 2001, 2002a). The model is a hydrostatic primitive equation model formulated in Cartesian coordinates in the horizontal plane with  $\sigma$  (pressure normalized by the surface pressure) vertical coordinate. The model consists of 21 layers in the vertical from  $\sigma = 0$  to  $\sigma = 1$  with higher resolutions in the planetary boundary layer (PBL). The layer interfaces are placed at  $\sigma = 0.0, 0.04, 0.07, 0.09, 0.11, 0.14, 0.17, 0.21, 0.27, 0.35, 0.45, 0.55, 0.65, 0.74, 0.82, 0.88, 0.93, 0.96, 0.984, 0.994$ , and  $1.0$ . The model physics include an  $E-\epsilon$  turbulence closure scheme for subgrid-scale vertical mixing above the surface layer (Langland and Liou 1996), a modified Monin–Obukhov scheme for the surface-flux calculations (Fairall et al. 1996), an explicit treatment of mixed ice phase cloud microphysics (Wang 1999, 2001), and a fourth-order horizontal diffusion with a deformation-dependent diffusion coefficient. The model prognostic variables consist of zonal and meridional winds; surface pressure; temperature; turbulence kinetic energy and its dissipation rate; and mixing ratios of water vapor, cloud water, rainwater, cloud ice, snow, and graupel. This model has been used for studies of various aspects of tropical cyclones (e.g., Wang et al. 2001; Wang 2002b,c).

Although TCM3 provides movable mesh and triply nested capabilities, we use a single mesh with a uniform grid spacing of 30 km to reduce the potential mesh interface effect on the structure of the wave train. The horizontal mesh consists of  $271 \times 201$  grid points, covering an area of 8100 by 6000 km centered at  $18^\circ\text{N}$ . A strong damping is specified in a sponge layer near the model lateral boundaries to minimize artificial wave reflection into the model interior. At this resolution, the mass-flux convective parameterization scheme (Tiedtke 1989) is used to calculate the effect of subgrid-scale cumulus convection.

### b. Initial conditions

Since our goal is to understand the internal dynamics of 3D energy dispersion of mature TCs, we focus on the evolution of TCs on a beta plane in a quiescent environment. The prescribed initial axisymmetric vortex has a radial and vertical tangential wind profile as follows:

$$V_t = \begin{cases} \frac{3\sqrt{6}}{4} V_m \left(\frac{r}{r_m}\right) \left[1 + \frac{1}{2} \left(\frac{r}{r_m}\right)^2\right]^{-(3/2)} \sin\left[\frac{\pi}{2} \left(\frac{\sigma - \sigma_u}{1 - \sigma_u}\right)\right], & \text{for } \sigma > \sigma_u; \\ 0, & \text{for } \sigma \leq \sigma_u, \end{cases}$$

TABLE 1. List of major numerical experiments.

Experiment symbol	Descriptions
CTL	Moist process; beta plane
DRY	Dry process; beta plane
Beta_High	Moist process; beta ( $f$ ) plane above (below) $\sigma = 0.3$
Beta_Low	Moist process; $f$ (beta) plane above (below) $\sigma = 0.3$

where  $r$  is the radial distance from the vortex center,  $V_m$  is the maximum tangential wind at the radius of  $r_m$ , and  $\sigma_u = 0.1$ . Therefore, the initial cyclonic vortex has a maximum azimuthal wind of  $30 \text{ m s}^{-1}$  at a radius of 100 km at the surface, decreasing gradually upward to zero at about 100 hPa. Given the wind fields, the mass and thermodynamic fields are then obtained based on a nonlinear balance equation so that the initial vortex satisfies both the hydrostatic and gradient wind balances (Wang 2001). The resting environment has a constant surface pressure of 1007.5 hPa. The initial water vapor mixing ratio and the environmental sounding are assumed to be horizontally homogeneous and to have the vertical profile of the January monthly mean at Willis Island, northeast of Australia (Holland 1997). This is representative of tropical ocean conditions in the southern Pacific tropical cyclone formation region. The sea surface temperature is fixed at  $29^\circ\text{C}$ . A detailed description of this numerical model and the initial conditions can be found in Wang (1999).

The major numerical experiments are listed in Table 1. The control experiment (CTL) is a case with diabatic

heating on the beta plane. The DRY experiment is a case in which the diabatic heating is turned off after 2-day integration. The Beta\_High and Beta\_Low are cases where the beta effect is included only in the upper and the lower troposphere, respectively. By comparing the CTL with the other cases, we will investigate the roles of vertical coupling between the upper and lower levels and the diabatic heating in the formation of 3D Rossby wave train. Each experiment is integrated for 10 days.

### 3. Structure and evolution features of the simulated 3D wave train

In the CTL experiment, after an initial drop in the maximum wind due to the lack of a boundary layer of the initial vortex, a rapid intensification occurs up to 36 h. During this early stage, to satisfy the mass continuity, the lower-level convergences result in a strong upper-level divergent anticyclonic circulation. In the early stage, the upper-level anticyclone is nearly symmetric, but the pattern becomes more complicated as the integration proceeds. The resulting circulation contains a cyclonic core and a trailing anticyclone with an extended, equatorward outflow jet. Accompanying the model TC northwestward movement, the isobars are elongated westward, forming an elliptic outer structure and an east–west asymmetry. A wave train with alternating cyclonic–anticyclonic–cyclonic circulations in the wake of the TC becomes apparent by day 5, and reaches a mature stage around day 10. The simulated wave train pattern in the mid–low troposphere (Fig. 1)

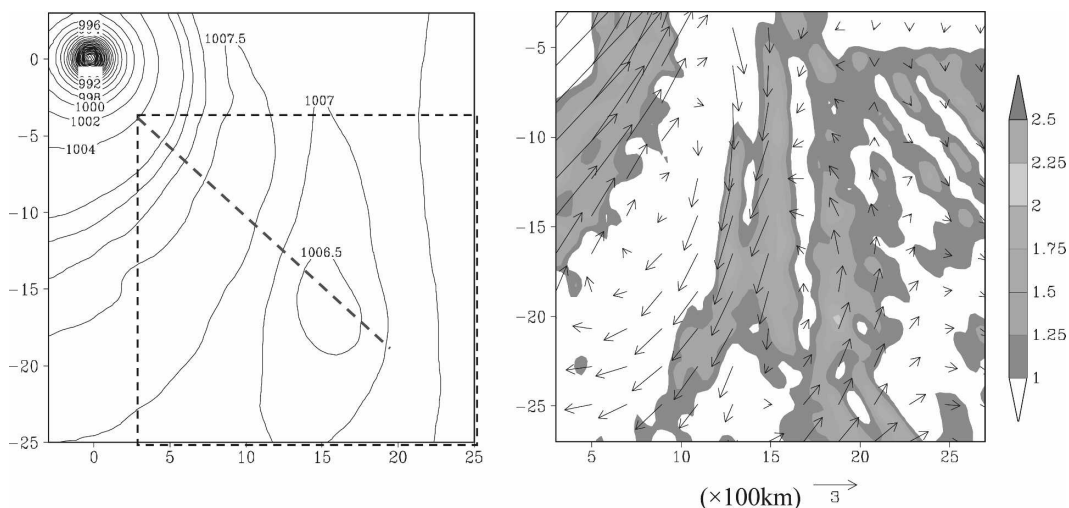


FIG. 1. (left) Surface pressure field (hPa) and (right) 850-hPa wind and vertical mean cloud mixing ratio (shaded;  $10^{-1} \text{ g kg}^{-1}$ ) pattern of a Rossby wave train in the box area shown in left panel at day 10. Horizontal distance is in increments of 100 km.

bears many similarities to those retrieved from the QuikSCAT observations (Li and Fu 2006). For instance, the alternating cyclonic and anticyclonic circulations are orientated in a northwest–southeast direction in the wake of the mature TC. Another noticeable characteristic of the wave train is its larger meridional scale than its zonal scale (Li et al. 2003). The wave train has a wavelength of 2000–2500 km. As Frank (1982) pointed out, the most common location of a new storm is about 20° to the southeast of a preexisting storm in the western North Pacific. This implies that the wavelength of Rossby wave train is approximately 2000 km, which agrees fairly well with our model results.

The simulated cloud liquid water (right panel of Fig. 1) pattern also bears a strong resemblance to observations during the course of wave train development (Li and Fu 2006). That is, an alternating cloudy–clear–cloudy pattern corresponds well to the alternating cyclonic–anticyclonic–cyclonic circulation. Convective cloud bands are collocated with the cyclonic circulation region, indicating a positive feedback between the diabatic heating and the low-level rotational circulation. Closer examination shows that several mesoscale eddies occur in the cyclonic vorticity region (not shown). These mesoscale vortices (~100 km in size) may have a significant impact on the formation of a new TC through either vortex merging (Simpson et al. 1997; Hendricks et al. 2004) or axisymmetrization (Möller and Montgomery 1999, 2000).

The vertical structure of the TCED-induced Rossby wave train is presented in Fig. 2. Note that clear Rossby wave trains appear in both the upper and lower troposphere, with minimum amplitude occurring in the midtroposphere ( $\sigma = 0.4$ ). This vertical structure differs somewhat from that derived from the NCEP–NCAR reanalysis by Li and Fu (2006), who pointed out that the northwest–southeast-oriented wave trains are evident from the surface to 500 hPa, and become less organized in the upper troposphere (200 hPa). Such difference is likely attributed to the much weaker TC intensity and outflow jet in the reanalysis products. Here the numerical simulation shows a noticeable baroclinic wave train structure with an out-of-phase relationship above and below  $\sigma = 0.4$ . Namely, an alternation of anticyclonic–cyclonic–anticyclonic (cyclonic–anticyclonic–cyclonic) circulation occurs in the upper (lower) levels. The generation of the baroclinic Rossby wave train results primarily from the baroclinic TC structure induced by the diabatic heating. The upper-level wave branch has a larger amplitude but is shallower than the lower-level counterpart, which is mainly because of the shallower anticyclonic outflow layer in the upper troposphere.

To illustrate the temporal evolution of the Rossby

wave train, we display the time sequence of the vertical–radius profiles of relative vorticity fields along a northwest–southeast-oriented axis (i.e., the dashed line in the left panel of Fig. 1, roughly the axis of the wave train) following the TC motion (Fig. 3). To highlight the Rossby wave train in the wake, the vertical–radius cross section is presented only from the radial distance of 500–3000 km away from the TC center. Initially, a weak positive relative vorticity perturbation develops in the upper troposphere ( $\sigma = 0.15$ ). This positive perturbation intensifies and extends gradually both outward and downward. For instance, the region of relative vorticity greater than  $0.5 \times 10^{-5} \text{ s}^{-1}$  (shaded area) reaches the PBL at day 7. Thereafter, a positive vorticity (PV) perturbation centers at a radius of 2200 km in the PBL, coinciding with the low-level cyclonic circulation region of the Rossby wave train (Fig. 2). The vorticity perturbations in the southeast quadrant appear to tilt northwestward with height. As a result, a first-baroclinic mode vertical structure appears in the wave train.

Similar downward development features appear in the kinetic energy [ $\text{KE} = (u^2 + v^2)/2$ ; as shown in Fig. 4] and PV fields. For example, a KE maximum center associated with an upper-tropospheric outflow jet initially occurs at  $\sigma = 0.15$ , then extends progressively both outward and downward (the center does not move outward). The outward and downward energy propagation will lead to a tilting of the maximum KE band toward the TC center with height.

The evolution of the relative humidity (RH) associated with the Rossby wave train is displayed in Fig. 5. The mid–low-level RH is little disturbed before day 6. Thereafter, a deep moist layer with high RH develops rapidly over the positive vorticity region of the wave train. For example, the 50% contour of RH reaches  $\sigma = 0.3$  in the cyclonic circulation region at day 10. This deep moist layer is primarily attributed to the enhanced convective activities, since the cyclonic vorticity at the PBL may enhance upward moisture transport through Ekman pumping. The enhanced convective heating may further intensify the low-level cyclonic vorticity within the Rossby wave train.

The time sequence of relative vorticity in the northwest quadrant is also examined. Similar to the southeast quadrant, a maximum vorticity perturbation occurs in the upper level (Fig. 6). However, there is no downward penetration of the vorticity, and no lower-level Rossby wave train develops. The preferred southeast quadrant for the wave train development is attributed to the asymmetry of the Rossby wave energy propagation (Chan and Williams 1987; Luo 1994). Li et al. (2003) argued that the larger (smaller) meridional (zonal) length scale of the wave train is essential for the

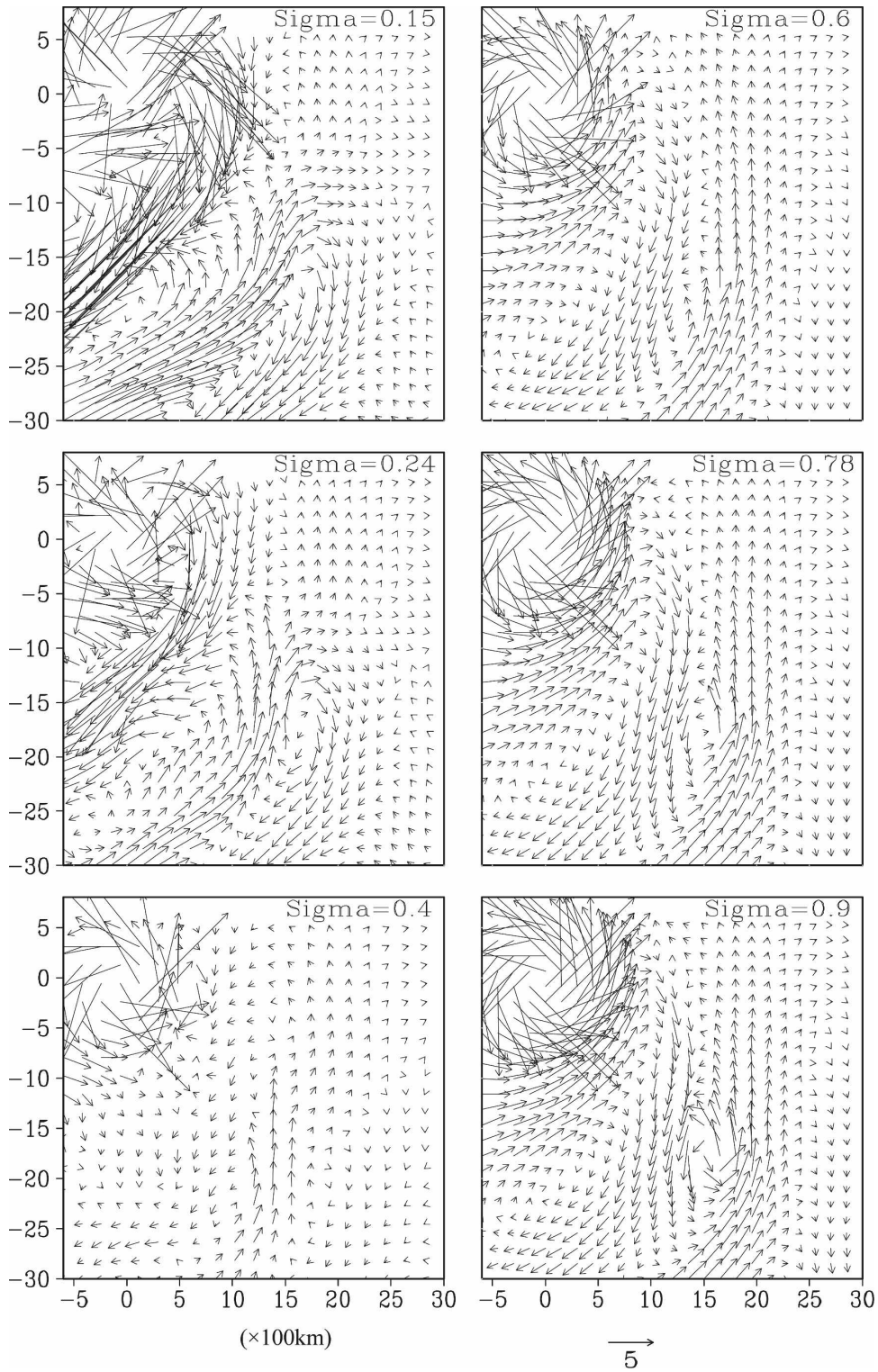


FIG. 2. Wind fields at different sigma levels at day 10; (0, 0) denotes the TC center.

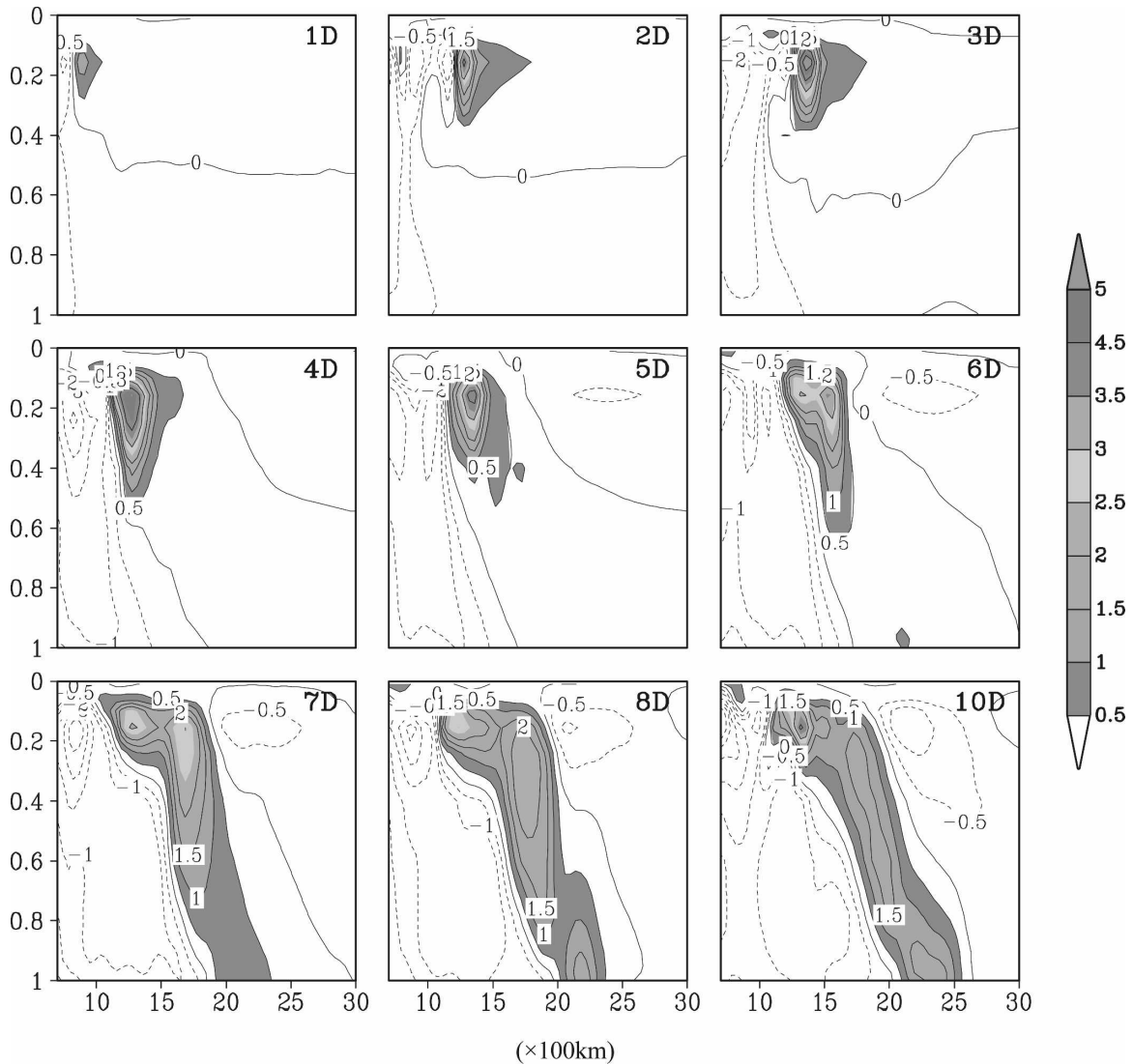


FIG. 3. Time evolution of vertical-radial cross sections of relative vorticity ( $10^{-5} \text{ s}^{-1}$ ) along the northwest–southeast axis (i.e., the dashed line in the left panel of Fig. 1). The number at the upper-right corner of each panel indicates the model time (1D denotes day 1).

southeastward energy propagation. Based on the Rossby wave dispersion relationship, wave energy propagates eastward when the meridional wavelength exceeds the zonal wavelength, and an opposite sign of the zonal and meridional wavenumber (corresponding to a northwestward phase speed) leads to a southward energy propagation component. The combination of these two factors leads to southeastward energy propagation. The southeastward energy dispersion is clearly demonstrated in terms of the time–radius cross section of KE (Fig. 7). The KE at both upper and lower levels propagates southeastward, radiating away from the TC center. Note that in the upper level, a secondary KE

maximum center develops much faster (day 1) compared with that in the lower level (about day 6).

To summarize, while the basic features of the lower-level wave train resemble those derived from the barotropic dynamic framework, new features associated with 3D TCED are revealed. That is, a positive vorticity perturbation associated with an outflow jet is generated first in the upper levels, followed by a downward propagation. Given the complex 3D energy dispersion characteristics, the following questions need to be addressed: What results in the asymmetric upper-level outflow jet? What role does this outflow jet play in the development of the lower-level wave train? And what

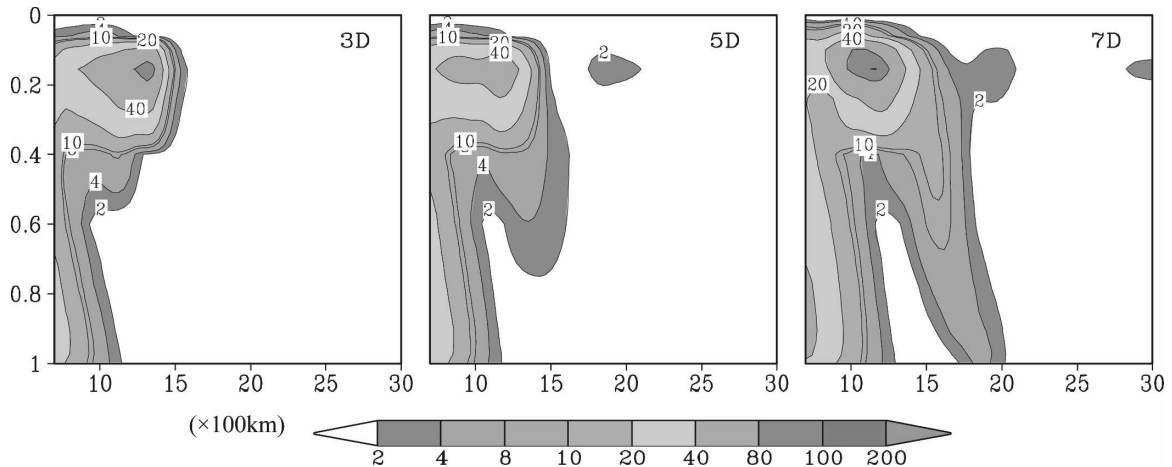


FIG. 4. Same as Fig. 3 but for kinetic energy ( $m^2 s^{-2}$ ).

causes the vertical tilting of the Rossby wave train? These questions are explored in the subsequent sections.

**4. Development of an asymmetric outflow jet**

The TCED-induced Rossby wave train essentially consists of beta-induced asymmetric circulations. Com-

pared with the barotropic vortex, one salient feature in the baroclinic TC is the more complex upper-level circulation. Figure 8 illustrates how an upper outflow jet is generated. In the early stage, the upper-level circulation is approximately symmetric. It is the energy dispersion that leads to the development of an asymmetric intense outflow jet in the southeast quadrant. Slightly outside of this outflow jet is a narrow belt of positive

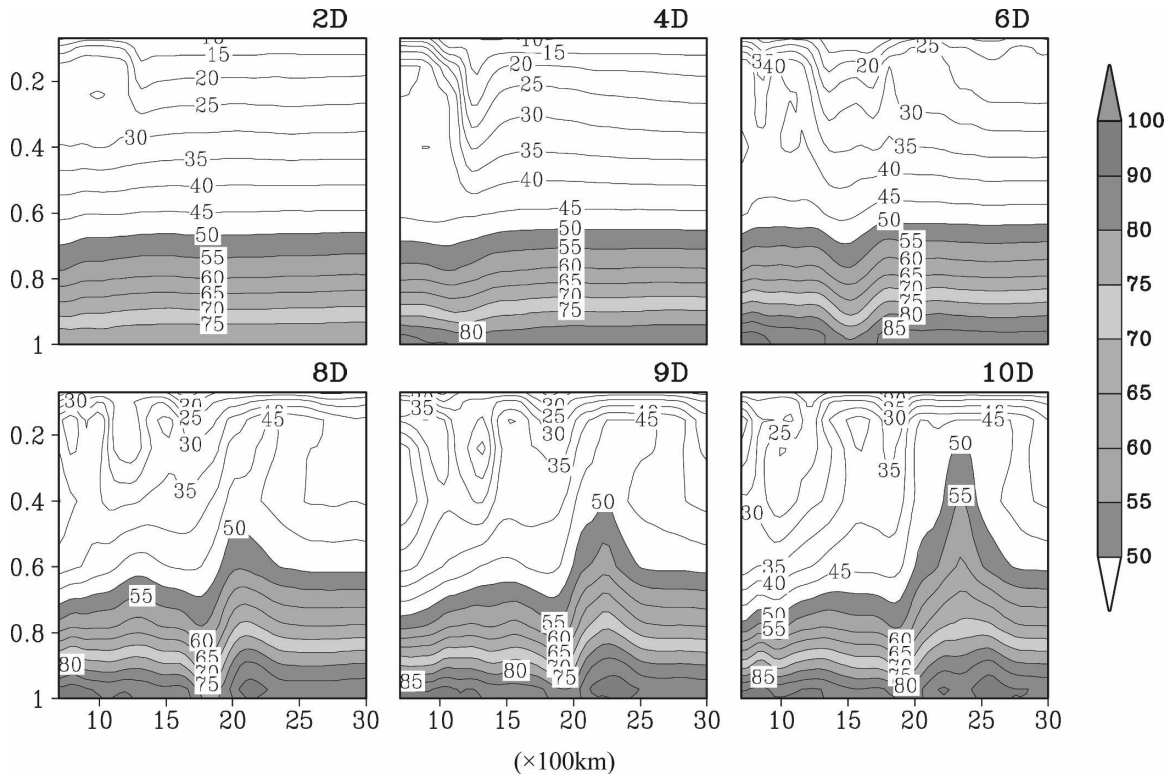


FIG. 5. Same as Fig. 3 but for relative humidity fields (%).

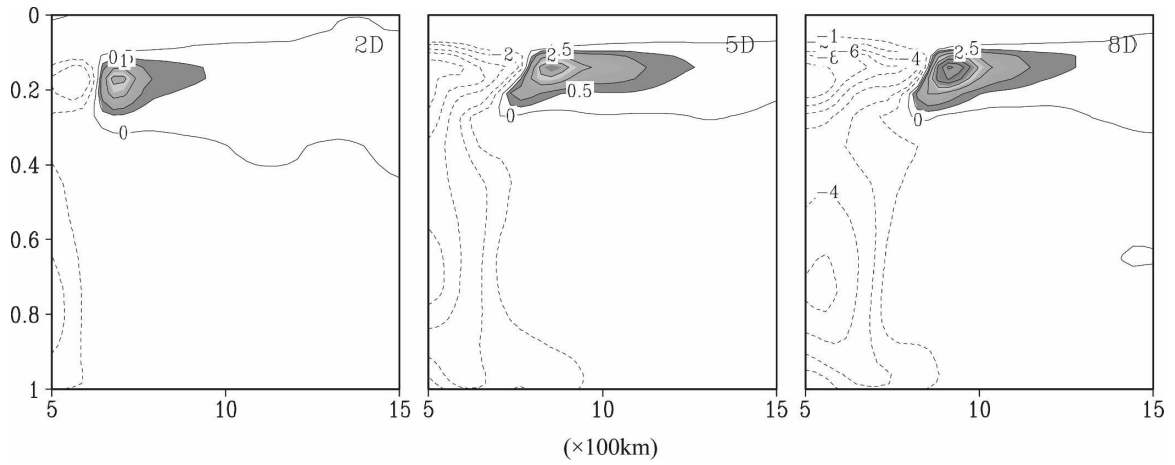


FIG. 6. Same as Fig. 3 but in the northwest quadrant.

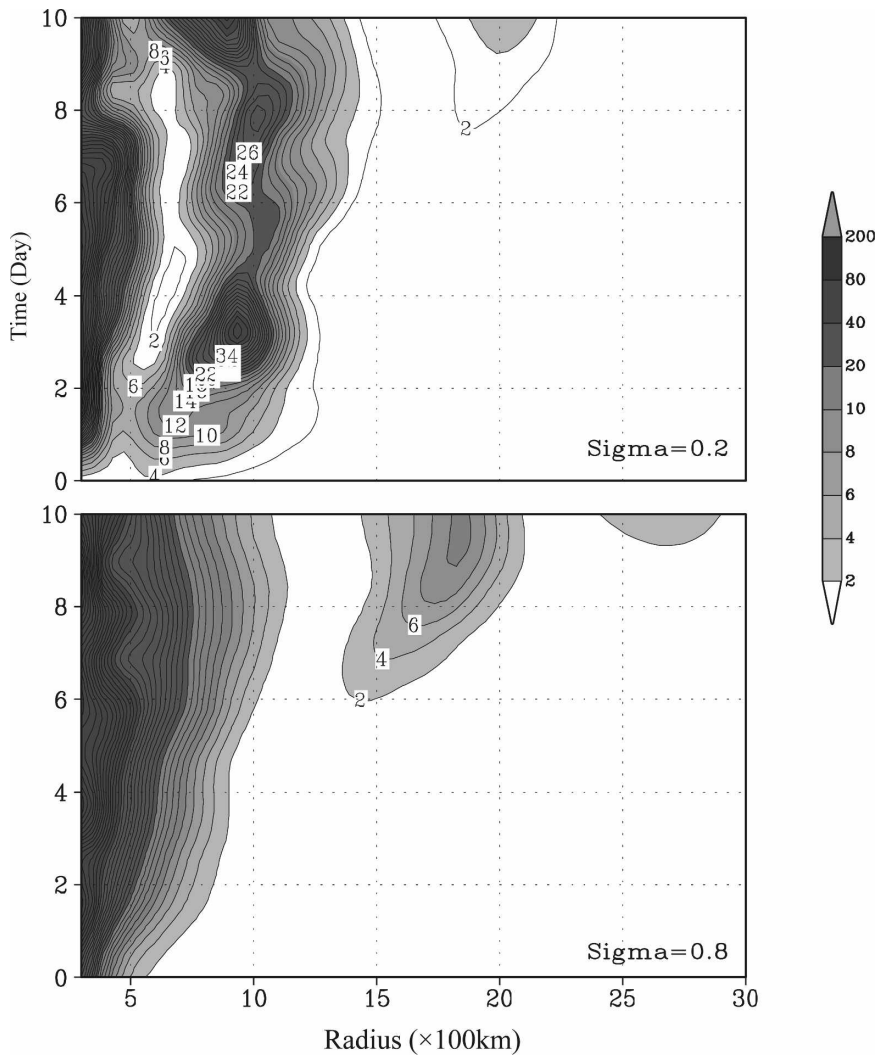


FIG. 7. The time–radius section of KE ( $m^2 s^{-2}$ ) in the upper ( $\sigma = 0.2$ ) and lower ( $\sigma = 0.8$ ) levels along a southeastward axis (the dashed line in Fig. 1).

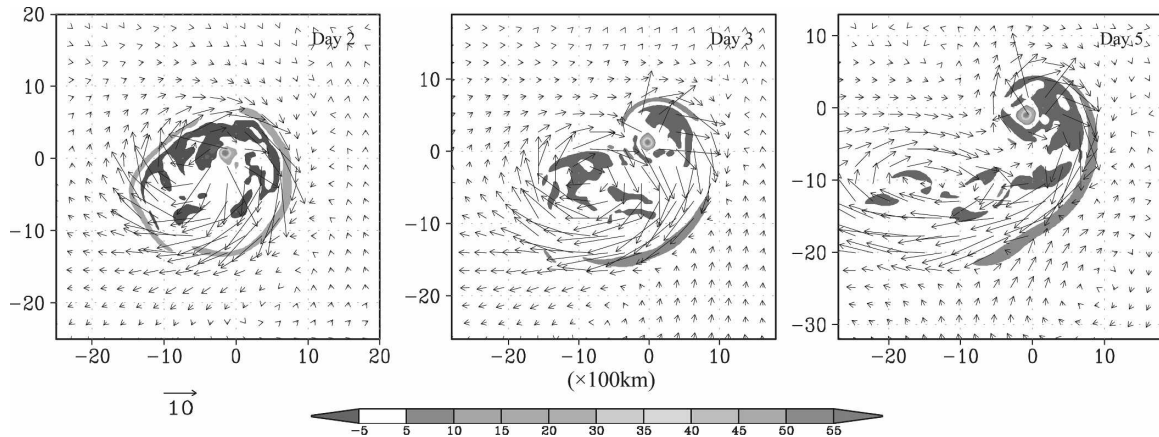


FIG. 8. The time evolution of the upper-outflow-layer ( $\sigma = 0.15$ ) circulation. From left to right: wind and relative vorticity (shaded) fields at days 2, 3, and 5.

vorticity. This upper outflow jet is confined within a shallow layer between  $\sigma = 0.1$  and  $0.3$ , with maximum amplitude at  $\sigma = 0.15$  (about 150 hPa, Fig. 4).

The TC outflow channel has been documented in previous observational (Black and Anthes 1971; Frank 1982) and numerical studies (Shi et al. 1990; Shapiro 1992; Wang and Holland 1996a,b). The establishment of the outflow asymmetries might be attributed to the combination of inertial, barotropic, and baroclinic instabilities (Anthes 1972; Kurihara and Tuleya 1974; Merrill 1984) or related to divergence patterns associated with prevailing environmental flow (Sadler 1978). An alternative interpretation, as discussed below, is based on Rossby wave dynamics. A TC may be considered to comprise a package of Rossby waves with different wavelengths (Chan and Williams 1987). The wave dispersion relationship shows faster westward phase speeds for longer waves than for shorter waves. As a result, the streamlines are stretched to the west while compressed to the east of the TC center. Based on the argument above, we give an alternative interpretation of the establishment of the outflow jet. The enhanced (reduced) pressure gradient force associated with the compressing (stretching) of the streamlines leads to an increase (decrease) of the wind speed to the east (west) of the TC center. Meanwhile, the upper-tropospheric anticyclonic flows advect the wavenumber-1 asymmetric flows, resulting in a northwest-southeast-oriented asymmetric flow pattern (Shapiro 1992; Wu and Emanuel 1993, 1994). The upper-level anticyclonic flows also cause a decrease in the inertial stability. As a result, the outflow jet extends to a much greater horizontal distance, especially to the equatorward side where the inertial stability is weak. The upper-level asymmetric circulations develop much more significantly compared with those in the lower levels.

The strong horizontal wind shear outside of this outflow jet core leads to positive cyclonic shear vorticity (Fig. 3). To this point, the initial development of the upper-level maximum vorticity and KE perturbation is ascribed to this outflow jet.

### 5. Impacts of the upper-level jet on 3D energy dispersion

In section 3, we illustrate the different evolution features of upper and lower wave branches. For a baroclinic vortex, away from the TC core region, the tangential wind decreases with height and radius, and the inertial stability decreases both outward and upward. Hence, the upper-level asymmetric circulation develops more rapidly and extends further outward, especially equatorward, because of lower inertial stability associated with the anticyclonic flow and the smaller Coriolis parameter. On the other hand, the stronger lower-level cyclonic flows result in a much larger inertial instability, thus the circulations are less asymmetric and more concentrated in the TC core region (Smith and Montgomery 1995). Therefore, the weaker (stronger) inertial instability may lead to faster (slower) development of the upper (lower)-level wave branch, which may partly account for the downward development shown in section 3.

For the 3D TCED, key questions are how the upper- and lower-level wave trains are related and what role the outflow jet plays in the formation of lower-level wave trains. To address these questions, two additional experiments are designed (see Table 1). In Beta\_High, we specify a beta plane ( $f$  plane) above (below)  $\sigma = 0.3$ . In Beta\_Low, an  $f$  plane (beta plane) is applied above (below)  $\sigma = 0.3$ . The turning point of  $\sigma = 0.3$  is chosen because the outflow layer is usually confined above this

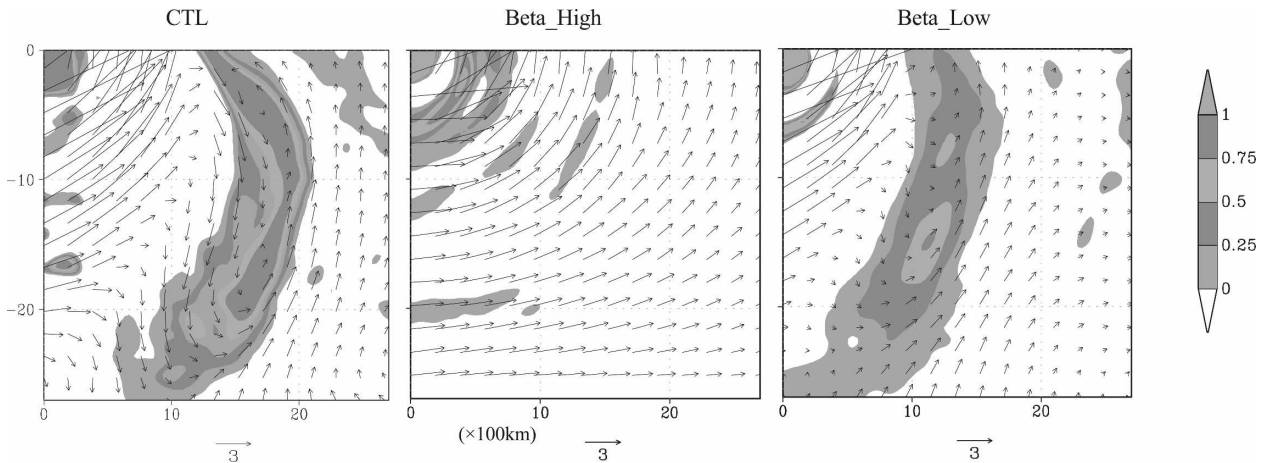


FIG. 9. Low-level ( $\sigma = 0.9$ ) circulations in the CTL, Beta\_High, and Beta\_Low experiments at day 6. Areas with positive relative vorticity are shaded.

level. Further sensitivity experiments show that as long as the turning point is between  $\sigma = 0.3$  and  $0.5$ , the results are qualitatively similar. By specifying an upper-level  $f$  plane, the asymmetric outflow jet may be removed so that the upper-tropospheric influence is suppressed. By specifying an  $f$  plane below  $\sigma = 0.3$ , it is possible to filter out the lower-level barotropic Rossby wave energy dispersion while retaining the asymmetric upper-level outflow jet. Therefore, by comparing these two experiments with CTL, it may be possible to learn the relative roles of the upper and lower asymmetric circulations in the formation of the 3D Rossby wave train.

Figure 9 displays the lower-level wave train patterns at day 6 in these three experiments. The Rossby wave train pattern is hardly discernible in Beta\_High, whereas it is clearly presented in both CTL and Beta\_Low, although the strength of the wave train is much greater in CTL. The difference among these three experiments can be further demonstrated in terms of the PV fields (Fig. 10). In CTL, wave trains with an alternating PV trough and ridge appear at both the upper and lower level. In Beta\_Low, a weaker lower-level wavelike pattern is identified. The upper-level PV is approximately symmetric about the TC center, indicating no upper wave train. In Beta\_High, along with an upper-level asymmetric outflow jet and its associated PV perturbation band, the upper-level wave is obvious in the southeast quadrant. However, the lower-level PV is nearly symmetric and is confined within the TC core region, and thus no lower-level wave exists. The results indicate the importance of the beta effect in the generation of the wave train.

The difference in the strength of wave trains between CTL and Beta\_Low is likely ascribed to the upper-level influence. That is, an intense asymmetric outflow jet

exists in CTL, whereas there is no such an entity in Beta\_Low. It has been realized that the outflow jet may affect the TC intensity (Black and Anthes 1971; Frank 1977; Merrill 1988; Rappin 2004). As shown in Fig. 11, the TC intensity [represented by central minimum sea level pressure (MSLP)] is much weaker in Beta\_Low than in CTL. For instance, the MSLP is 970 hPa (945 hPa) in Beta\_Low (CTL) at day 6. A comparison of the azimuthally mean tangential winds ( $\sigma = 0.9$ ) reveals that both the TC strength and size are larger in CTL as well. It suggests that a near-symmetric upper-level flow leads to a weaker TC (Beta\_Low), and an asymmetric outflow jet favors a more intense TC (CTL). TCED depends greatly on the TC size and structure (Flierl et al. 1983; Chan and Williams 1987; Carr and Elsberry 1995) and intensity (Li and Fu 2006). Therefore, a weaker Rossby wave train in Beta\_Low is likely due to the weaker TC intensity and smaller size in the absence of an upper-level outflow jet. It is consistent with the composite study by Merrill (1988), who summarized the outflow-layer differences between intensifying and nonintensifying hurricanes (see their Fig. 11) and found that the outflow layer with an “open” (closed) streamline pattern corresponds to intensifying (nonintensifying) cases. To assert that the weaker TC is due to the absence of the beta effect-induced asymmetric outflows, an additional  $f$ -plane simulation is conducted. The result shows that the simulated TC in Beta\_High has a stronger tangential wind ( $\sim 52 \text{ m s}^{-1}$ ) than that in the  $f$ -plane simulation ( $\sim 45 \text{ m s}^{-1}$ ). Meanwhile, the beta-plane storm has a relatively larger size than the  $f$ -plane storm. This supports our claim that the upper-level outflow may influence the TC intensity and size. In Emanuel (1986), the TC secondary circulation is treated as an idealized Carnot heat engine where en-

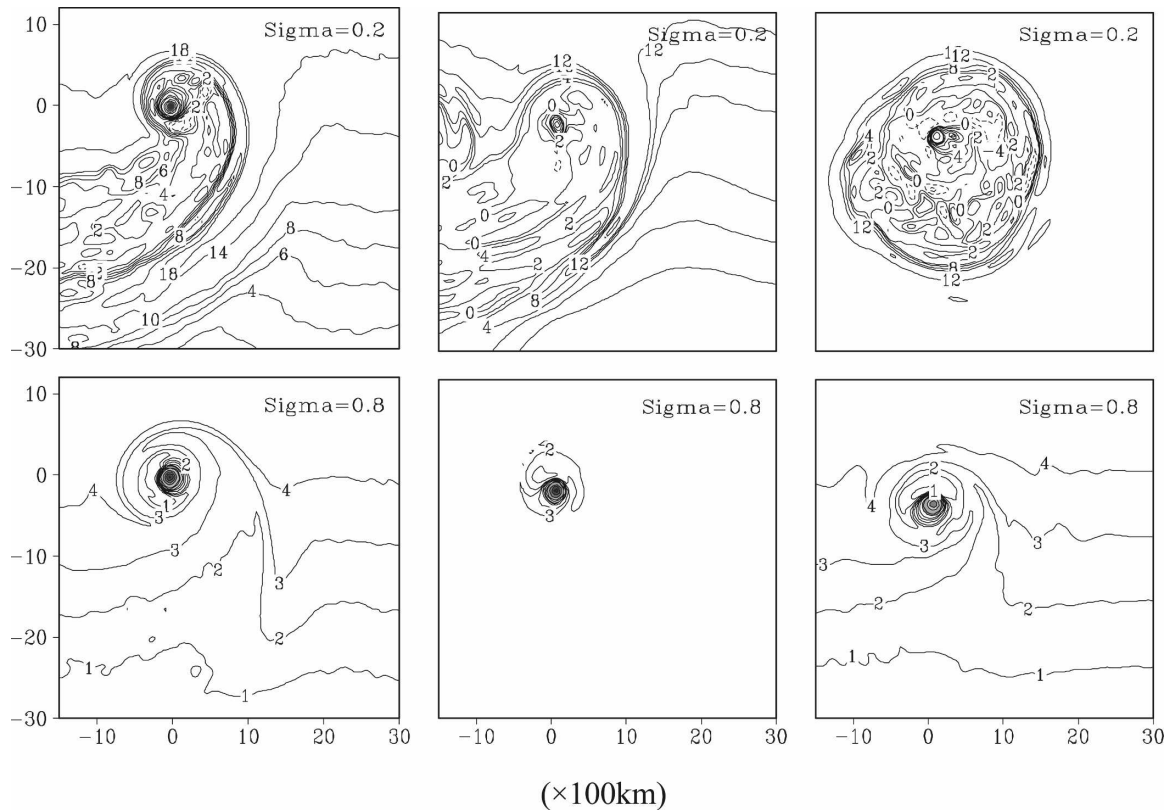


FIG. 10. The PV fields in (left) CTL [0.1 potential vorticity units (PVU); 1 PVU  $\equiv 10^{-6} \text{ m}^2 \text{ s}^{-1} \text{ K kg}^{-1}$ ], (middle) Beta\_High, and (right) Beta\_Low at day 6.

ergy input by air–sea interaction is balanced by frictional dissipation in the boundary layer and outflow layer (energy is drained as the outflow anticyclone expands against the ambient cyclonic rotation of the environment). Rappin (2004) suggested symmetric expansion led to large energy expenditures that were manifested in large anticyclonic kinetic energies. Asymmetric expansion into regions of weak resistance led to small energy expenditures and therefore small anticyclonic kinetic energies. Thus, the smaller energy expenditures in Beta\_High may result in a stronger TC. However, how the asymmetric outflow jet influences the TC size through the extent of the secondary circulation is unclear.

To demonstrate the impact of the upper-tropospheric circulation on the energy dispersion, the Eliassen–Palm (E–P) flux is used to diagnose the wave energy propagation and wave–mean flow interaction (Schubert 1985; Molinari et al. 1995; Chen et al. 2003). Following Molinari et al. (1995), the E–P flux divergence in a potential temperature ( $\theta$ ) vertical coordinate is written as

$$\nabla \cdot \mathbf{F} = -\frac{1}{r} \frac{\partial}{\partial r} r^2 \overline{(\sigma u_L)' v_L'} + \frac{\partial}{\partial \theta} \overline{p' \frac{\partial \psi'}{\partial \lambda}},$$

where  $\mathbf{F} \equiv \{-r \overline{(\sigma u_L)' v_L'}, \overline{p' [\partial \psi' / (\partial \lambda)]}\}$  is the E–P flux vector, which is calculated on cylindrical coordinates, and the overbar represents the azimuthal mean. Here  $\sigma = -\partial p / (\partial \theta)$  is the pseudodensity;  $u_L'$  and  $v_L'$  are the storm-relative radial and tangential winds, respectively;  $\psi'$  is the Montgomery streamfunction; and  $\lambda$  is the azimuthal angle. The radial component of the E–P flux represents the eddy angular momentum flux, while the vertical component is the eddy heat flux. Parallel to the wave group velocity, the E–P flux vectors illustrate the wave energy propagation.

Figure 12 shows the radius– $\theta$  cross sections of E–P flux vectors and their divergence averaged from days 3–5 for the three experiments. In both CTL and Beta\_High, the greatest eddy activities appear on the 355-K surface near the radius of outflow jet, indicating the dominant eddy angular momentum fluxes in the upper level. Much weaker wave activities exist at the same  $\theta$  surface in Beta\_Low. Meanwhile, the largest  $\nabla \cdot \mathbf{F}$  occurs in CTL and Beta\_High at the 700-km radius, where the anticyclonic outflow is the strongest. This implies that eddy activities are closely related to the development of the upper-level outflow jet. The larger upper-level E–P flux vector implies that the upper wave

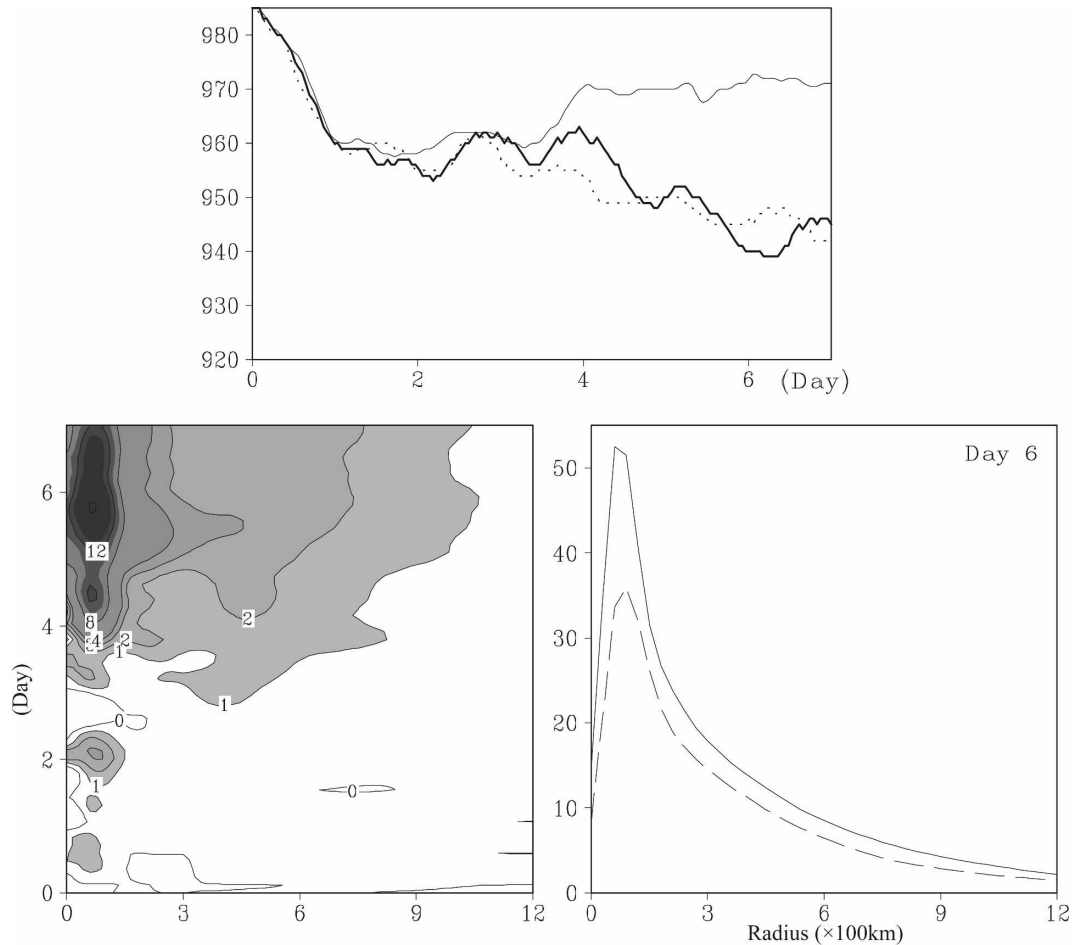


FIG. 11. (top) Time evolutions of MSLP (hPa) in CTL (thick solid), Beta\_High (dotted), and Beta\_Low (thin solid), and (bottom left) difference in the symmetric tangential winds between CTL and Beta\_Low (CTL minus Beta\_Low) and (bottom right) tangential wind profile for CTL (solid line) and Beta\_Low (dashed line) at day 6 ( $\text{m s}^{-1}$ ).

branch has a larger energy propagation speed than that of the lower level, which is consistent with faster (slower) development of the upper- (lower)-level wave train. As expected, the slower response in the lower levels may partially explain the downward development. Of particular interest is a significant difference in the lower-level energy propagation between CTL and Beta\_High. In CTL, below the outflow layer (say  $\theta = 355$  k), the E-P flux indicates both outward and downward energy propagation. In Beta\_High, the E-P flux shows weak downward propagation from the outflow layer, and no horizontal energy propagation exists in the lower level in the absence of the beta effect. By the same reason, much weaker upper-level eddy activities are observed in the Beta\_Low as the beta effect is excluded there. No vertical component of the E-P flux vectors can be identified in the mid-low troposphere, indicating no downward energy propagation.

Nevertheless, the lower-level beta effect induces outward energy propagation (bottom panel of Fig. 12), which agrees well with the barotropic Rossby wave dynamics.

The results above suggest that the generation of a 3D Rossby wave train cannot be fully explained by pure barotropic dynamics. In addition to outward barotropic energy dispersion, a baroclinic TC upper-outflow-layer circulation will induce downward energy propagation. Therefore, both outward and downward energy propagation will result in the downward-tilted development of the Rossby wave train (Fig. 4). While the barotropic dynamics of the beta effect is essential for the generation of Rossby wave trains, the upper-level outflow jet may further enhance the lower-level wave trains. For example, in Beta\_Low, the wave train cannot develop fully without the upper-level influence. Given that the E-P flux applied here only describes the azimuthal

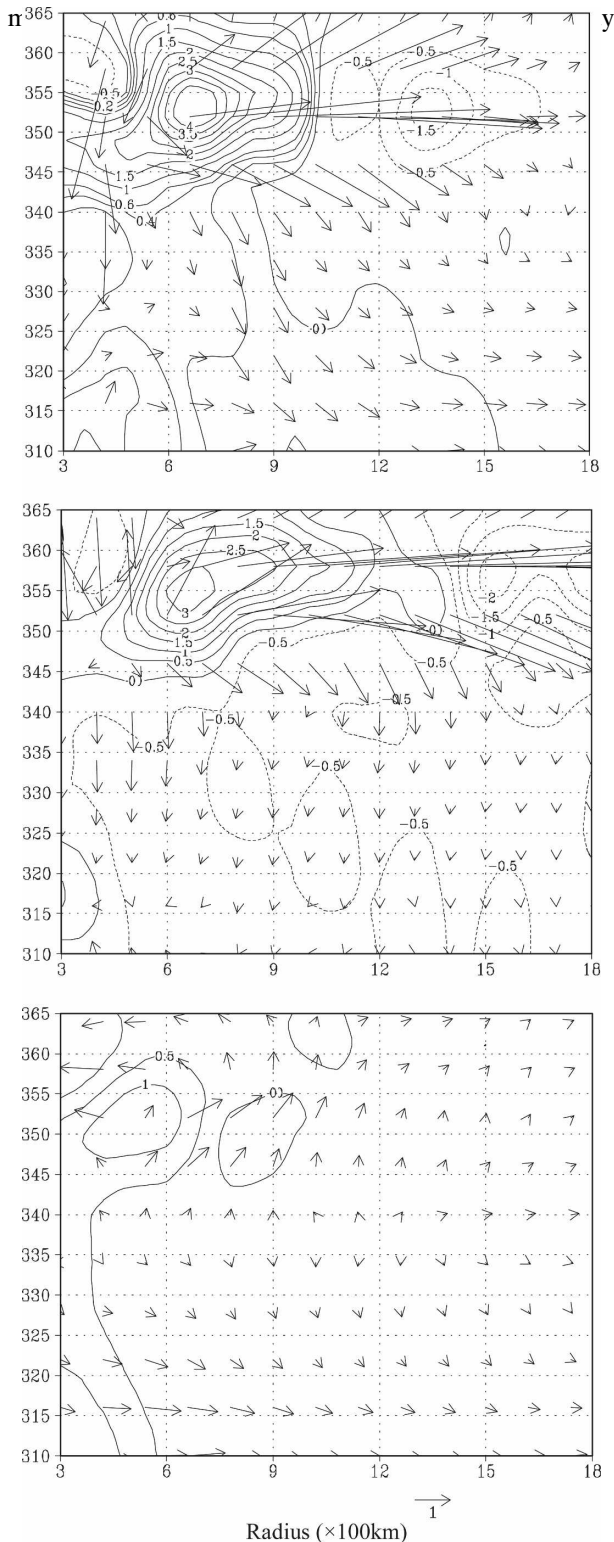


FIG. 12. Potential temperature-radius cross sections of E-P flux vectors and their divergence averaged from days 3–5 (contours;  $0.5 \times 10^4 \text{ Pa m}^2 \text{ K}^{-1} \text{ s}^{-2}$ ) for (top) CTL, (middle) Beta\_High, and (bottom) Beta\_Low. The horizontal and vertical components are scaled by  $1 \times 10^{-9}$  and  $1 \times 10^{-5}$ , respectively.

underestimate the wave activity flux in the southeast quadrant. Despite this weakness, comparisons of the wave activities in these three experiments help provide insight into how the upper-tropospheric circulation influences the 3D Rossby wave train.

## 6. Roles of diabatic heating

In this section, we will examine the role of diabatic heating in the TCED process. It is well realized that the convective heating plays a major role in maintaining the TC circulation system with cyclonic vorticity below and anticyclonic vorticity aloft. The evolution of a diabatic vortex could substantially differ from that of an adiabatic one (Wang and Li 1992; Wang and Holland 1996a). Given that TCED is sensitive to the vertical structure of a TC, the sensitivity of the energy dispersion characteristics to turning off the diabatic heating is now investigated. A DRY experiment is designed in which certain model physics schemes are turned off after 48 h and the integration continues for another 6 days. The model physics schemes turned off include a convective parameterization scheme, an explicit mixed-phase cloud microphysics package, an  $E$ -turbulence closure scheme for subgrid-scale vertical mixing above the surface layer, a modified Monin–Obukhov scheme for the surface-flux calculation, and the surface friction.

Figure 13 displays the simulated Rossby wave train at day 5 (three days after diabatic heating is turned off). A clear lower-level wave train with alternating cyclonic–anticyclonic–cyclonic circulations appears in the wake, whereas such a feature is hardly identified at the same time in CTL. It indicates that the wave train forms much faster in the absence of the diabatic heating. Meanwhile, a significant difference between CTL and DRY is the evolution of the outflow-layer circulation. After initially spinning up, the vortex has the same structure as that of CTL at day 2. An upper outflow jet is generated and stretches from the vortex core to several hundred kilometers to the southwest. Once diabatic heating is turned off, the outflow jet decays rapidly (Fig. 13). This suggests that the diabatic heating will maintain the outflow jet against the energy dispersion. Figure 14 compares the vertical and radial profiles of azimuthally mean tangential and radial winds between CTL and DRY. As expected, there is no clear upper-level anticyclonic circulation in the DRY experiment. Furthermore, the lower-level maximum tangential wind is about  $40 \text{ m s}^{-1}$  in CTL but only  $25 \text{ m s}^{-1}$  in DRY at day 4, whereas the radius of maximum wind increases from 90 km in CTL to 150 km in DRY. The

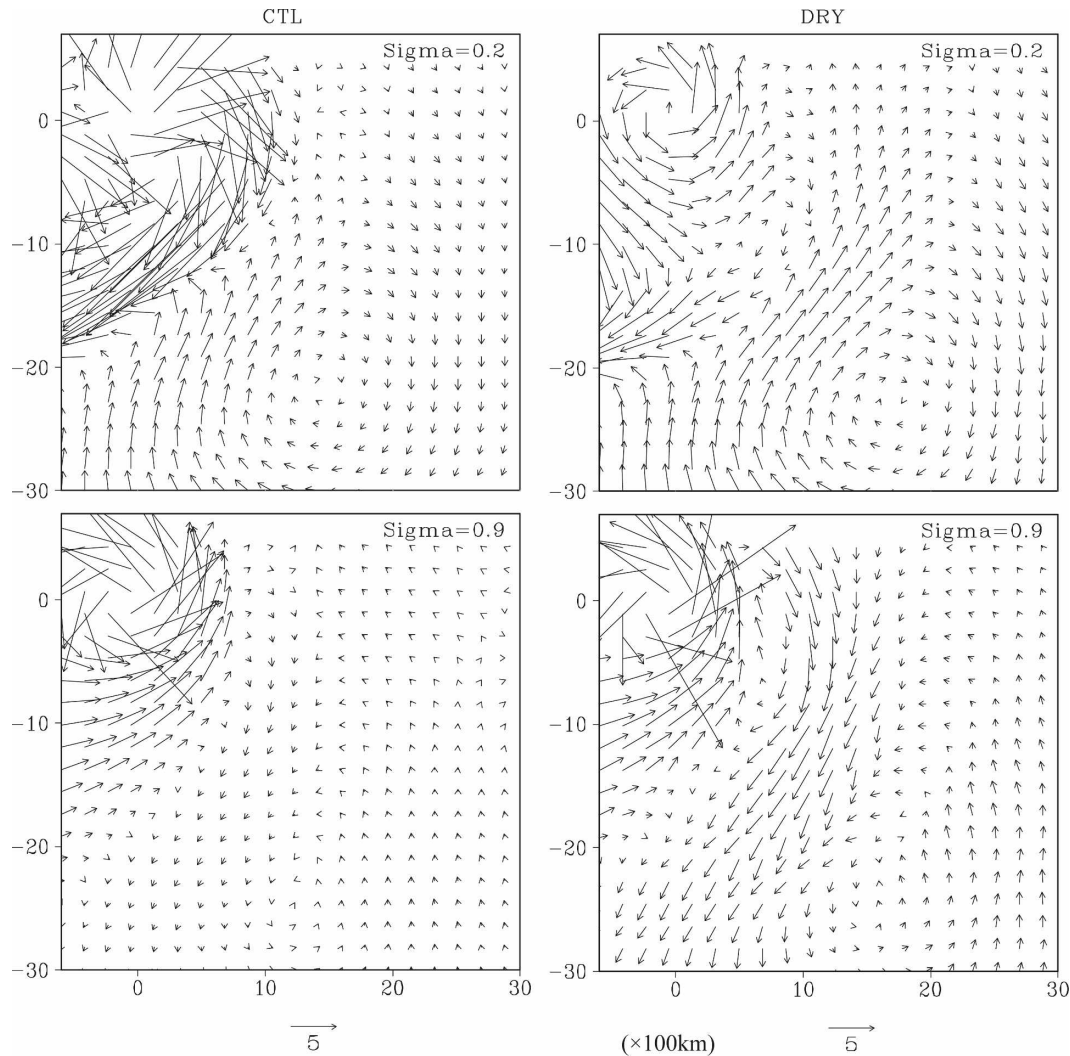


FIG. 13. Simulated wind fields in the (left) CTL and (right) DRY experiments at day 5.

weakening in the primary circulation is accompanied by the suppressed secondary circulation.

The following two factors may explain the earlier development of the Rossby wave train in DRY. One is related to change of the TC inflow in the outer region. As we know, the inflow may modulate the Rossby wave group velocity through a “Doppler shift” effect. Although significant low-level radial inflow occurs within a few hundred kilometers of the center, weak inflow (i.e.,  $-0.25 \text{ m s}^{-1}$ ) is still present in the outer region ( $\sim 2000 \text{ km}$ ) in CTL. In sharp contrast, no significant radial inflow is found in DRY. As the Rossby wave energy disperses southeastward, the group velocity is opposite to the mean radial inflow  $V_r$  in the lower troposphere. As a result, the total group velocity  $C_g + V_r$  will be reduced in the southeast quadrant. Given the stronger low-level inflow in CTL, the total group ve-

locity would be smaller, indicating slower energy propagation and thus a longer period for the development of the low-level wave train in CTL than in DRY.

Second, previous nondivergent barotropic studies have shown that the energy dispersion is more sensitive to the size of a vortex rather than its intensity (e.g., Carr and Elsberry 1995). With the sudden vanishing of the diabatic heating, the TC secondary circulation collapses rapidly and is accompanied by a decrease in maximum tangential wind and an increase in the radius of maximum wind. According to Carr and Elsberry (1995), the extent to which the vortex resists asymmetric forcing is proportional to  $V_{\text{max}}/R_{\text{max}}^2$  (here  $V_{\text{max}}$  is the maximum tangential wind at the radius of  $R_{\text{max}}$ ). Given that  $V_{\text{max}}$  is 40 (25)  $\text{m s}^{-1}$  and  $R_{\text{max}}$  is 90 (150) km in CTL (DRY), the value of  $V_{\text{max}}/R_{\text{max}}^2$  is  $4.9 \times 10^{-9} \text{ m}^{-1} \text{ s}^{-1}$  in CTL,

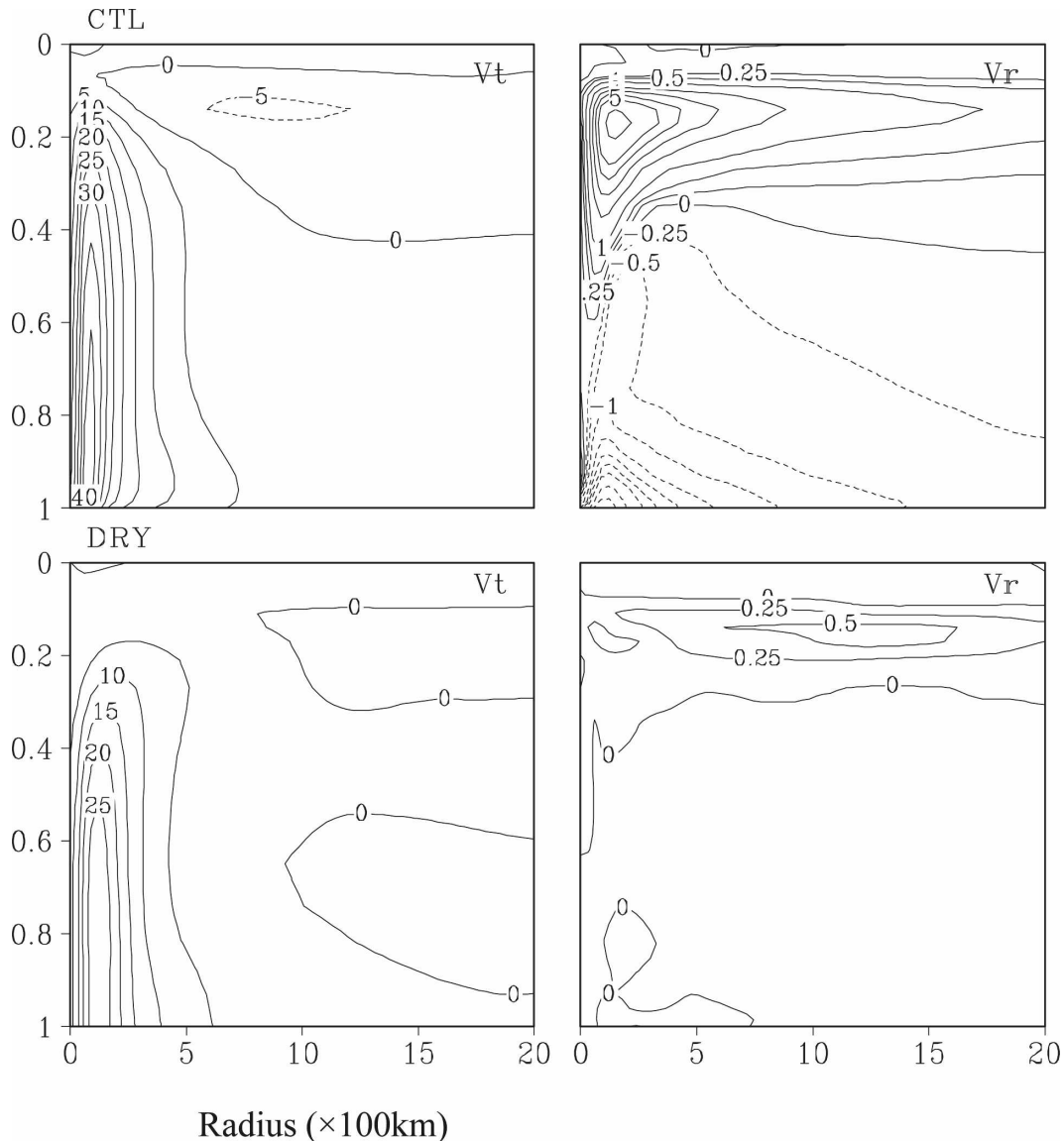


FIG. 14. The vertical–radial cross sections of the symmetric components of tangential and radial winds ( $\text{m s}^{-1}$ ) at day 4 in the CTL and DRY experiments.

which is nearly 4 times larger than that in DRY ( $1.1 \times 10^{-9} \text{ m}^{-1} \text{ s}^{-1}$ ). Therefore, the vortex in DRY is more susceptible to the beta-induced dispersion and thus a faster establishment of the wave train.

To further examine this size effect, we conduct two additional Beta\_Low experiments with no diabatic processes. The initial vortex has a maximum wind of  $30 \text{ m s}^{-1}$  at a radius of  $100 \text{ km}$  in the first experiment and a weaker intensity ( $V_{\text{max}} = 20 \text{ m s}^{-1}$ ) at a larger radius of  $300 \text{ km}$  in the second experiment (see the upper panel of Fig. 15). The bottom panel of Fig. 15 displays the simulated low-level Rossby wave trains at day 4. It is clear that the Rossby wave train is significantly stron-

ger in the case with a larger TC size, supporting the argument above.

## 7. Conclusions

Previous studies on TC energy dispersion were confined to a barotropic framework. In this study, we applied a baroclinic model to examine the characteristics of 3D TCED-induced Rossby wave trains in a quiescence environment. While a baroclinic TC moves northwestward because of the beta effect, Rossby waves emit energy southeastward. This leads to the formation of a synoptic-scale wave train in its wake. The

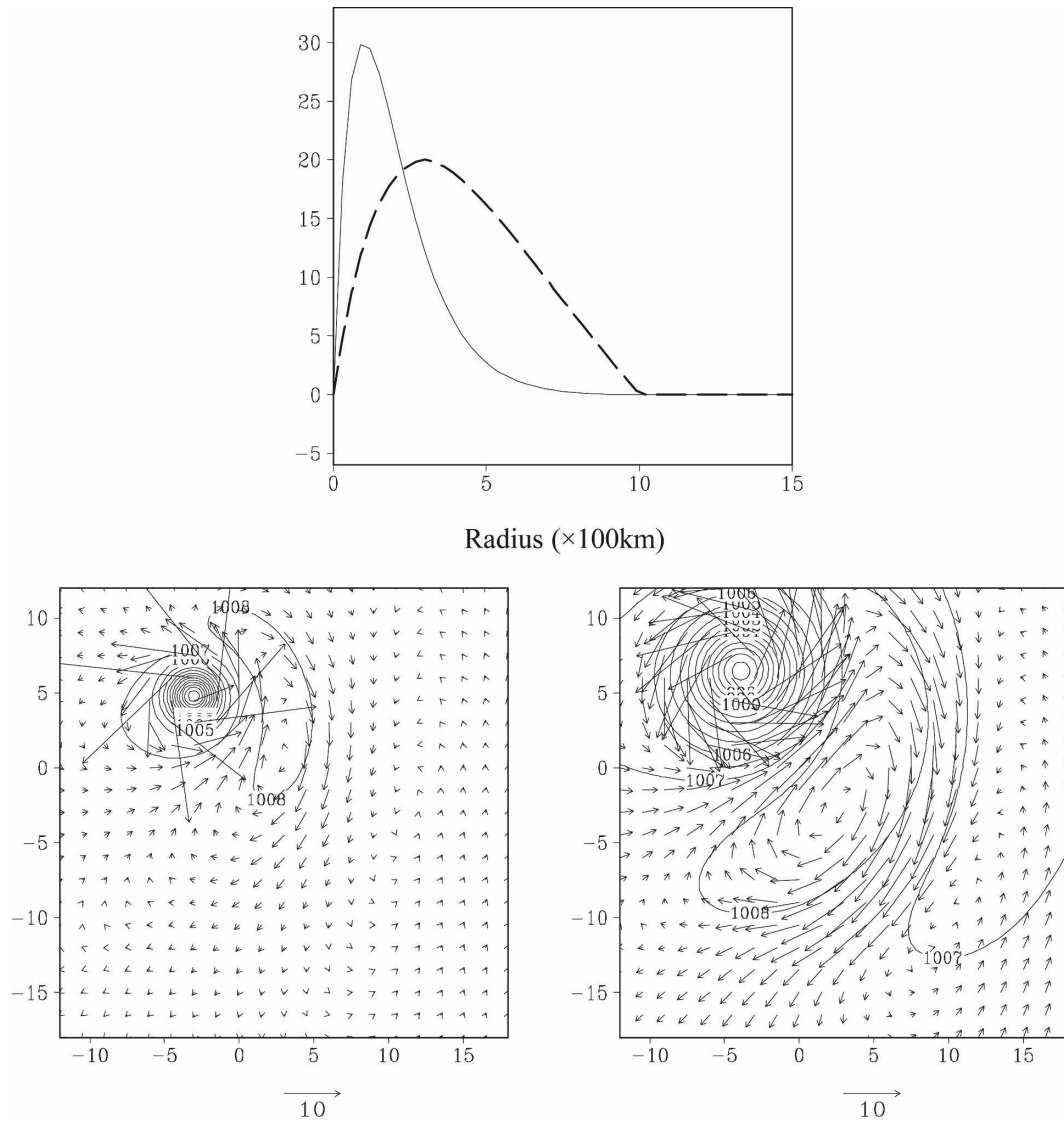


FIG. 15. (top) The initial tangential wind profiles for a TC with stronger intensity but smaller size (solid line) and a TC with larger size but weaker intensity (dashed line), and (bottom) the simulated Rossby wave trains at day 4 in the two cases: (left) the stronger intensity case; (right) the larger-size case.

simulated 3D wave train exhibits a noticeable baroclinic structure with alternating cyclonic–anticyclonic–cyclonic (anticyclonic–cyclonic–anticyclonic) circulation in the lower (upper) level.

A noteworthy feature associated with the 3D TCED is the downward propagation of the relative vorticity and kinetic energy. This evolution feature is beyond the 2D barotropic dynamics, and possible mechanisms responsible for this 3D TCED-induced Rossby wave train are illustrated in Fig. 16. Because of the vertical differential inertial stability, the upper-level wave train develops faster than the lower-level counterpart. As a result, an intense asymmetric outflow jet is established in

the upper level. This beta effect–induced strong asymmetry in the upper level may further influence the lower-level Rossby wave train through the following two processes. On one hand, the outflow jet triggers downward energy propagation, leading to the strengthening of the lower-level Rossby wave train. On the other hand, it exerts an indirect effect on the lower-level wave train strength by changing the TC intensity and structure.

To investigate the relative role of the lower-level Rossby wave energy dispersion and the upper-tropospheric impact, two sensitivity experiments (Beta\_High and Beta\_Low) are conducted. In Beta\_Low, the upper

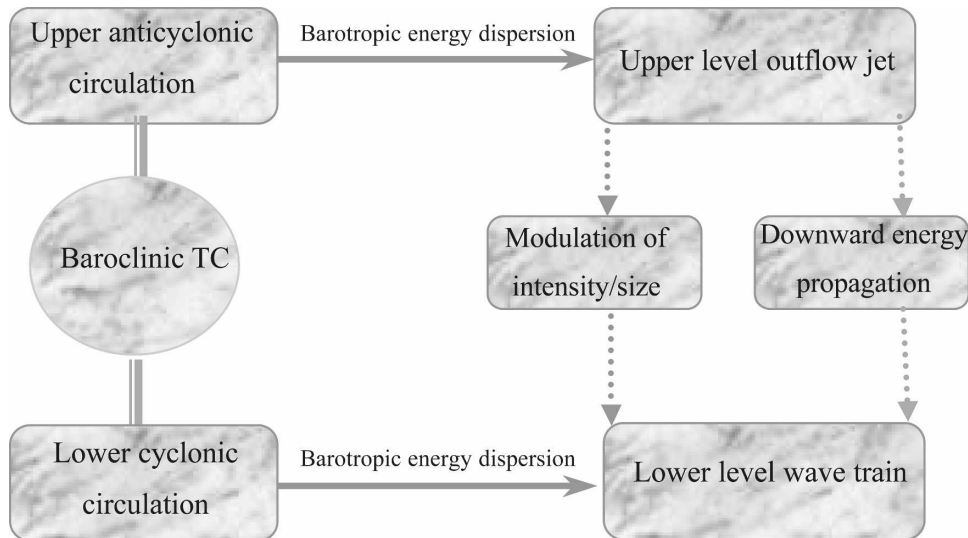


FIG. 16. Schematic diagram illustrating possible mechanisms responsible for the 3D Rossby wave train development. The thick solid arrows indicate barotropic Rossby wave dynamics, and the dotted arrows indicate the influence of the upper-tropospheric circulation.

asymmetric outflow jet is filtered out by excluding the upper-level beta effect. As a result, the downward energy propagation is hardly discerned and the lower-level wave train is much weaker. In Beta\_High, the lower-level wave train is hardly identified when the lower-level beta effect is excluded. The comparison of the control and sensitivity experiments above reveals that the development of the upper asymmetric outflow jet results in a more intense TC with a relatively larger size. This further strengthens the lower-level Rossby wave train, as the energy dispersion is sensitive to the TC intensity and size (Carr and Elsberry 1995). The numerical results indicate that barotropic Rossby wave dynamics is essential for the lower-level wave train development, while the upper-tropospheric asymmetry due to the beta effect has a significant additional impact. The 3D TC energy dispersion illustrates more complicated characteristics than the conventional 2D barotropic dynamics.

A further sensitivity experiment reveals that a sudden removal of diabatic heating may result in an increase of  $R_{\max}$  and a significant reduction of the lower-level inflow, both of which favor the initial wave train development. As discussed above, the increase of the TC size may enhance the energy dispersion. Meanwhile, the Rossby wave group velocity may be modulated by the TC inflow through the Doppler shift effect.

In the current study, we examine the TCED in a quiescent environment. The investigation of 3D Rossby wave train development in idealized and realistic background flows is currently in progress and the results will be reported elsewhere.

**Acknowledgments.** We thank Dr. Liguang Wu and two anonymous reviewers for their constructive comments. This work was supported by NRL Grant N00173061G031 and ONR Grants N000140710145 and N000140210532. International Pacific Research Center is partially sponsored by the Japan Agency for Marine-Earth Science and Technology (JAMSTEC).

#### REFERENCES

- Anthes, R. A., 1972: Development of asymmetries in a three-dimensional numerical model of the tropical cyclone. *Mon. Wea. Rev.*, **100**, 461–476.
- , 1982: *Tropical Cyclones—Their Evolution, Structure and Effects*. Meteor. Monogr., No. 41, Amer. Meteor. Soc., 208 pp.
- Black, P. G., and R. A. Anthes, 1971: On the asymmetric structure of the tropical cyclone outflow layer. *J. Atmos. Sci.*, **28**, 1348–1366.
- Briegel, L. M., and W. M. Frank, 1997: Large-scale influences on tropical cyclogenesis in the western North Pacific. *Mon. Wea. Rev.*, **125**, 1397–1413.
- Carr, L. E., III, and R. L. Elsberry, 1995: Monsoonal interactions leading to sudden tropical cyclone track changes. *Mon. Wea. Rev.*, **123**, 265–290.
- Chan, J. C. L., and R. T. Williams, 1987: Analytical and numerical studies of the beta-effect in tropical cyclone motion. Part I: Zero mean flow. *J. Atmos. Sci.*, **44**, 1257–1265.
- Chen, Y., G. Brunet, and M. K. Yau, 2003: Spiral bands in a simulated hurricane. Part II: Wave activity diagnostics. *J. Atmos. Sci.*, **60**, 1239–1256.
- Davidson, N. E., and H. H. Hendon, 1989: Downstream development in the Southern Hemisphere monsoon during FGGE/WMONEX. *Mon. Wea. Rev.*, **117**, 1458–1470.
- Emanuel, K., 1986: An air-sea interaction theory for tropical cyclones. Part I: Steady-state maintenance. *J. Atmos. Sci.*, **43**, 585–605.

- Fairall, C. W., E. F. Bradley, D. P. Rogers, J. B. Edson, and G. S. Young, 1996: Bulk parameterization of air-sea fluxes for Tropical Ocean-Global Atmosphere Coupled-Ocean Atmosphere Response Experiment. *J. Geophys. Res.*, **101**, 3747–3764.
- Flierl, G. R., 1984: Rossby wave radiation from a strongly nonlinear warm eddy. *J. Phys. Oceanogr.*, **14**, 47–58.
- , M. E. Stern, and J. A. Whitehead, 1983: The physical significance of modons: Laboratory experiments and general integral constraints. *Dyn. Atmos. Oceans*, **7**, 233–263.
- Frank, W. M., 1977: The structure and energetics of the tropical cyclone. I. Storm structure. *Mon. Wea. Rev.*, **105**, 1119–1135.
- , 1982: Large-scale characteristics of tropical cyclones. *Mon. Wea. Rev.*, **110**, 572–586.
- Hendricks, E. A., M. T. Montgomery, and C. A. Davis, 2004: The role of “vortical” hot towers in the formation of tropical cyclone Diana (1984). *J. Atmos. Sci.*, **61**, 1209–1232.
- Holland, G. J., 1995: Scale interaction in the western Pacific monsoon. *Meteor. Atmos. Phys.*, **56**, 57–79.
- , 1997: The maximum potential intensity of tropical cyclones. *J. Atmos. Sci.*, **54**, 2519–2541.
- Kurihara, Y., and R. E. Tuleya, 1974: Structure of a tropical cyclone developed in a three-dimensional numerical simulation model. *J. Atmos. Sci.*, **31**, 893–919.
- Langland, R. H., and C.-S. Liou, 1996: Implementation of an  $E-\epsilon$  parameterization of vertical subgrid-scale mixing in a regional model. *Mon. Wea. Rev.*, **124**, 905–918.
- Li, T., and B. Fu, 2006: Tropical cyclogenesis associated with Rossby wave energy dispersion of a preexisting typhoon. Part I: Satellite data analyses. *J. Atmos. Sci.*, **63**, 1377–1389.
- , —, X. Ge, B. Wang, and M. Peng, 2003: Satellite data analysis and numerical simulation of tropical cyclone formation. *Geophys. Res. Lett.*, **30**, 2122, doi:10.102a/2003GL018556.
- , X. Ge, B. Wang, and Y. T. Zhu, 2006: Tropical cyclogenesis associated with Rossby wave energy dispersion of a preexisting typhoon. Part II: Numerical simulations. *J. Atmos. Sci.*, **63**, 1390–1409.
- Luo, Z., 1994: Effect of energy dispersion on the structure and motion of tropical cyclone. *Acta Meteor. Sin.*, **8**, 51–59.
- McDonald, N. R., 1998: The decay of cyclonic eddies by Rossby wave radiation. *J. Fluid Mech.*, **361**, 237–252.
- Merrill, R. T., 1984: Structure of the tropical cyclone outflow layer. *Proc. 15th Conf. on Hurricanes and Tropical Meteorology*, Miami, FL, Amer. Meteor. Soc., 421–426.
- , 1988: Environmental influences on hurricane intensification. *J. Atmos. Sci.*, **45**, 1678–1687.
- Molinari, J., S. Skubis, and D. Vollaro, 1995: External influences on hurricane intensity. Part III: Potential vorticity structure. *J. Atmos. Sci.*, **52**, 3593–3606.
- Möller, J. D., and M. T. Montgomery, 1999: Vortex Rossby waves and hurricane intensification in a barotropic model. *J. Atmos. Sci.*, **56**, 1674–1687.
- , and —, 2000: Tropical cyclone evolution via potential vorticity anomalies in a three-dimensional balance model. *J. Atmos. Sci.*, **57**, 3366–3387.
- Rappin, E. D., 2004: The role of environmental inertial stability in tropical cyclone intensification. Ph.D. thesis, University of Wisconsin—Madison, 106 pp.
- Ritchie, E. A., and G. J. Holland, 1999: Large-scale patterns associated with tropical cyclogenesis in the western Pacific. *Mon. Wea. Rev.*, **127**, 2027–2043.
- Sadler, J. C., 1978: Mid-season typhoon development and intensity changes and the tropical upper tropospheric trough. *Mon. Wea. Rev.*, **106**, 1137–1152.
- Schubert, W. H., 1985: Wave, mean-flow interactions, and hurricane development. Preprints, *16th Conf. on Hurricanes and Tropical Meteorology*, Houston, TX, Amer. Meteor. Soc., 140–141.
- Shapiro, L. J., 1992: Hurricane vortex motion and evolution in a three-layer model. *J. Atmos. Sci.*, **49**, 140–153.
- , and K. V. Ooyama, 1990: Barotropic vortex evolution on a beta plane. *J. Atmos. Sci.*, **47**, 170–187.
- Shi, J. J., W. S. Chang, and S. Raman, 1990: A numerical study of the outflow of tropical cyclones. *J. Atmos. Sci.*, **47**, 2042–2055.
- Simpson, J., E. Ritchie, G. J. Holland, J. Halverson, and S. Stewart, 1997: Mesoscale interactions in tropical cyclone genesis. *Mon. Wea. Rev.*, **125**, 2643–2661.
- Smith, G. B., and M. T. Montgomery, 1995: Vortex axisymmetrization and its dependence on azimuthal wavenumbers or asymmetric radial structure changes. *Quart. J. Roy. Meteor. Soc.*, **121**, 1615–1650.
- Tiedtke, M., 1989: A comprehensive mass flux scheme for cumulus parameterization in large-scale models. *Mon. Wea. Rev.*, **117**, 1779–1800.
- Wang, B., and X. Li, 1992: The beta drift of three-dimensional vortices: A numerical study. *Mon. Wea. Rev.*, **120**, 579–593.
- Wang, Y., 1999: A triply nested movable mesh tropical cyclone model with explicit cloud microphysics—TCM3. Bureau of Meteorology Research Centre Research Rep. 74, 81 pp.
- , 2001: An explicit simulation of tropical cyclones with a triply nested movable mesh primitive equation model: TCM3. Part I: Model description and control experiment. *Mon. Wea. Rev.*, **129**, 1370–1394.
- , 2002a: An explicit simulation of tropical cyclones with a triply nested movable mesh primitive equation model: TCM3. Part II: Some model refinements and sensitivity to cloud microphysics parameterization. *Mon. Wea. Rev.*, **130**, 3022–3036.
- , 2002b: Vortex Rossby waves in a numerically simulated tropical cyclone. Part I: Overall structure, potential vorticity, and kinetic energy budgets. *J. Atmos. Sci.*, **59**, 1213–1238.
- , 2002c: Vortex Rossby waves in a numerically simulated tropical cyclone. Part II: The role in tropical cyclone structure and intensity changes. *J. Atmos. Sci.*, **59**, 1239–1262.
- , and G. J. Holland, 1996a: Beta drift of baroclinic vortices. Part I: Adiabatic vortices. *J. Atmos. Sci.*, **53**, 411–427.
- , and —, 1996b: Beta drift of baroclinic vortices. Part II: Diabatic vortices. *J. Atmos. Sci.*, **53**, 3737–3756.
- , J. D. Kepert, and G. J. Holland, 2001: The effect of sea spray evaporation on tropical cyclone boundary layer structure and intensity. *Mon. Wea. Rev.*, **129**, 2481–2500.
- Wu, C.-C., and K. A. Emanuel, 1993: Interaction of a baroclinic vortex with background shear: Application to hurricane movement. *J. Atmos. Sci.*, **50**, 62–76.
- , and —, 1994: On hurricane outflow structure. *J. Atmos. Sci.*, **51**, 1995–2003.

Copyright of *Journal of the Atmospheric Sciences* is the property of *American Meteorological Society* and its content may not be copied or emailed to multiple sites or posted to a listserv without the copyright holder's express written permission. However, users may print, download, or email articles for individual use.